Nanofibers Formed Through π···π Stacking of the Complexes of Glucosyl-*C*2-salicyl-imine and Phenylalanine: Characterization by Microscopy, Modeling by Molecular Mechanics, and Interaction by α-Helical and β-Sheet Proteins

Amitabha Acharya, Balaji Ramanujam, Atanu Mitra, and Chebrolu P. Rao*

Department of Chemistry, Indian Institute of Technology Bombay, Powai, Mumbai -400 076, India

ABSTRACT This paper deals with the self-assembly of the 1:1 complex of two different amphiphiles, namely, a glucosyl-salicyl-imino conjugate (L) and phenylalanine (Phe), forming nanofibers over a period of time through π···π interactions. Significant enhancement observed in the fluorescence intensity of L at ~423 nm band and the significant decrease observed in the absorbance of the ~215 nm band are some characteristics of this self-assembly. Matrix-assisted laser desorption ionization/time of flight titration carried out at different time intervals supports the formation of higher aggregates. Atomic force microscopy (AFM), transmission electron microscopy, and scanning electron miscroscopy results showed the formation of nanofibers for the solutions of L with phenylalanine. In dynamic light scattering measurements, the distribution of the particles extends to a higher diameter range over time, indicating a slow kinetic process of assembly. Similar spectral and microscopy studies carried out with the control molecules support the role of the amino acid moiety over the simple —COOH moiety as well as the side chain phenyl moiety in association with the amino acid, in the formation of these fibers. All these observations support the presence of π···π interactions between the initially formed 1:1 complexes leading to the fiber formation. The aggregation of 1:1 complexes leading to fibers followed by the formation of bundles has been modeled by molecular mechanics studies. Thus the fiber formation with L is limited to phenylalanine and not to any other naturally occurring amino acid and hence a polymer composed of two different biocompatible amphiphiles. AFM studies carried out between the fiber forming mixture and proteins resulted in the observation that only BSA selectively adheres to the fiber among the three α-helical and two β-sheet proteins studied and hence may be of use in some medical applications.

KEYWORDS: 1-(D-glucopyranosyl-2′-deoxy-2′-iminomethyl)-2-hydroxy-benzene amphiphile · nanofibers · π···π interactions · MALDI · microscopy · molecular mechanics (MM+) · α-helical albumins · β-sheet lectins

Molecular self-assembly attracts a great deal of attention of scientists and technologists in recent times because of its use in the design and fabrication of nanostructures that lead to the development of advanced materials.[1,2] Among this, peptide amphiphiles (PAs), possessing both hydrophobic and hydrophilic segments[3] are one class of molecules that plays an important role in bioactivity and sensing studies.[4−6] These segments lead to ordered arrangements to minimize the interfacial energies with solvent to result in the formation of different nanoarchitectures, such as, spheres,[7] tubes,[8] and cylinders.[9,10] Because such molecular scaffolds are biocompatible, they present a great potential as self-assembling materials for drug delivery[11] and as bioactive scaffolds for cell signaling.[12] Some examples of this include (a) the formation of glyco-conjugate nanoribbons from the self-assembly of PAs possessing both the peptide moiety as well as the carbohydrate moiety;[13] (b) the architectural changes brought about in the formation of nanofibers of the PAs conjugated with polydiacetylenes upon photoirradiation;[3] (c) the formation of different architectures from hydrophilic dextran-derived polymers with cationic and anionic derivatizations;[14] and so on. The first example of this is the result of a π···π interaction exhibited between the phenyl moieties of the Phe residues of the neighbor molecules. The role of the aromatic side chain in the fiber formation of amyloids has already been reported in the literature.[15−17] Similarly, some carbohydrate derivatives were reported to form fibers when attached to aromatic side chains.[18,19] Though the formation of nanofibers was reported from the interaction of two different amphiphiles in the literature,[20−28] none of these is between a glycoconjugate and an amino acid. Therefore, this article deals with the formation of nanofibers from two different amphiphiles,

*Address correspondence to cprao@iitb.ac.in.

Received for review October 25, 2009 and accepted May 26, 2010.

Published online June 3, 2010.
10.1021/nn1006286

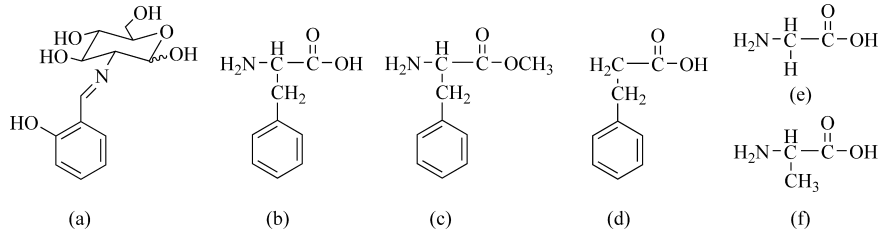

Figure 1. Schematic structures of the amphiphiles: (a) glucosyl-salicyl-imino conjugate (L) and (b) phenylalanine. Schematic structures of the control molecules: (c) methyl ester of phenylalanine (Phe-OMe), (d) 3-phenylpropionic acid, (e) glycine, and (f) alanine.

namely, Phe possessing a side chain phenyl moiety and a glucosyl-salicyl-imine conjugate possessing a salicyl moiety. To the best of our knowledge, this is the first report where two different biocompatible amphiphiles, a glycoconjugate and an amino acid, were shown to form nanofibers.

RESULTS AND DISCUSSION

The glucosyl-C2-salicyl-imine conjugate amphiphile, 1-(D-glucopyranosyl-2′-deoxy-2′-iminomethyl)-2-hydroxybenzene (L), possessing both hydrophilic carbohydrate moiety and the hydrophobic phenyl moiety, was synthesized by reacting glucosylamine hydrochloride with salicylaldehyde in a 1:1 ratio in the presence of 1.2 equivalents of triethylamine as base in one step in 87% yield. The L has been characterized by ^{1}H NMR, ESI-MS, and elemental analysis (Supporting Information, SI 01). The schematic structures of the amphiphiles, namely, L and phenylalanine, are shown in Figure 1, along with the control molecules used in the present study.

Fluorescence Titration Studies. When phenylalanine (Phe) is added to L in methanol (Experimental Section) and excited at 320 nm, the emission band emerges at ~435 nm owing to the presence of the imine moiety in conjunction with the aromatic moiety, as also found by us in the case of glyco- and calix-imino-conjugates.[29−35] The fluorescence intensity of the emission peak increases slowly as a function of time (Supporting Information, SI 02) (even after subtracting the background emission from Phe) as a result of the complexation enhanced fluorescence when the amino acid complexes with L. A total saturation in fluorescence intensity is attained over a period of 1 day (Figure 2a). With this, the overall enhancement in the fluorescence intensity was found to be (47 ± 5)-fold, though it is only (6 ± 1)-fold immediately when Phe was added to L. The enhancement in the fluorescence intensity has also been found to increase further when the mole ratio of the added Phe increases (Figure 2b) and attains saturation around ≥2 equivalents by exhibiting same enhancement ratio. Such fluorescence enhancement is expected only when Phe interacts with L, where the interactions can be either through hydrogen bonding or through hydrophobic (or π···π type) or through a combination of these.

To establish the involvement of −COOH, $-NH_2$, or phenyl moiety of Phe on the observed fluorescence enhancement, experiments were carried out with methyl ester of phenylalanine (Phe-OMe), 3-phenylpropionic acid (3-PPA), glycine (Gly), and alanine (Ala) (Figure 1). While it is the −COOH moiety that was converted to ester in Phe−OMe, it is the $-NH_2$ group that was replaced by −H in 3-PPA to study the importance of −COOH and $-NH_2$ moieties, respectively. On the other hand, the studies carried out using Gly and Ala, provides the importance of the side chain phenyl moiety present in Phe. The titrations carried out between L and Phe-OMe exhibited fluorescence enhancement similar to that observed in the titration of L with simple Phe suggesting that the −COOH present in Phe is not critical for the interaction (Figure 2c). Similar titrations carried out between L and 3-PPA resulted in no change in the fluorescence intensity of L, suggesting that the amine moiety present in Phe is indeed necessary for the interaction.

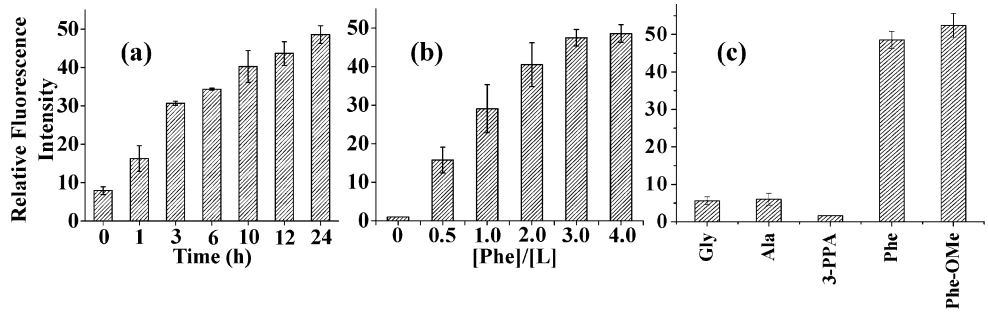

Figure 2. Relative fluorescence intensity observed during the titration of L with Phe: (a) as a function of time; (b) as a function of [Phe]/[L] mole ratio at 24 h. (c) Titration of L with different control molecules: Gly, Ala, 3-PPA, Phe, and Phe-OMe, and the fluorescence is at 24 h in all the cases.

Even the titrations carried out between L and Gly/Ala exhibited only *ca.* (6.0 ± 1.0)-fold change in the fluorescence intensity suggesting that the side chain phenyl moiety is indeed needed for exhibiting large fluorescence enhancement. All this indicates that though Gly or Ala can interact with L, the species formed in this case is much different from that formed between Phe and L. Thus the results obtained from the fluorescence studies seem to suggest the involvement of amine group in conjunction with the phenyl moiety present in Phe in forming the corresponding species responsible for the large fluorescence enhancement as that observed in the case of [L+Phe]. It would be only the amine moiety that is responsible in the case of Gly or Ala, and hence it brings only a marginal fluorescence increase as observed in the case of [L+Gly] or [L+Ala].

The fluorescence data fits well with a 1:1 complex formed through hydrogen-bond interactions involving the amine moiety of the amino acid in the case of Gly, Ala, and Phe. However, the complex formed initially seems to interact and/or aggregate through the phenyl moiety of Phe, which cannot happen in the case of Gly or Ala due to the absence of this moiety. Therefore, the possible presence of both the hydrogen bonding and the hydrophobic or the $\pi\cdots\pi$ interactions in the species formed in the case of [L+Phe] has been further addressed based on other experimental and computational studies as reported in this article.

MALDI Studies. The formation of the complex species between L and Phe followed by its growth was monitored by measuring the mass spectra of the solution of [L+Phe] by matrix-assisted laser desorption ionization (MALDI) at various time intervals. With increasing time, higher molecular weight species were formed at the cost of the initially formed 1:1 species. Thus, as a function of time, species were grown with *m/z* values in the range, 2220−2280, 2330−2400, 2420−2640, 2690−2810, and 3350−3500 Da, suggesting the growth of the aggregated species (Figure 3). The aggregations range from pentameric to hexameric to even octameric ones. The species observed at *m/z* values of 2234, 2372, and 2518 are suggestive of the pentameric species, 2729 denotes the hexameric, and that at 3445 denotes the octameric species. The intensity of the peak corresponding to the octamer indeed increased when measured after 24 h. Thus the MALDI titration results in providing evidence for the formation of oligomers of L with Phe, $[L+Phe]_n$, where *n* has been found at least in the range of 4−8.

Absorption Titration Studies. The growth of the initially formed 1:1 species has been further monitored by following the changes observed in the absorption spectra of the ~215 nm band (Experimental Section, Supporting Information, SI 03). No change in the absorbance was observed when L was titrated either with Gly or Ala, but considerable absorbance changes were observed in the titration of L with Phe. The trend observed in this

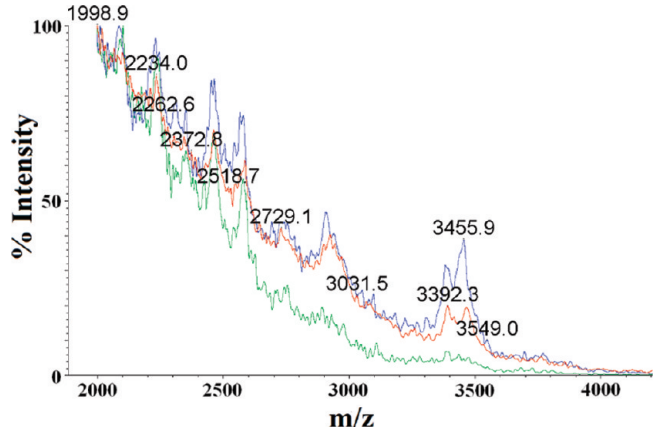

Figure 3. MALDI mass spectra measured from the solution of [L+Phe] at different time intervals: 1 h (green); 8 h (red); 24 h (blue).

data is suggestive of the role of the side chain phenyl moiety in exhibiting $\pi\cdots\pi$ interactions in the case of [L+Phe] and not with [L+Ala] or [L+Gly], as the same is not expected in the case of the latter owing to the absence of phenyl side chain moiety. However, the initial complex formed between L and the amino acid can be noticed from the absorbance changes observed with the 350 nm band. Thus the absorption studies not only confirmed the initial formation of the complex between L and the amino acid but also supported the growth of the species through $\pi\cdots\pi$ interactions in case of phenylalanine.

Prevention of Aggregation in the Presence of Ethidium Bromide (EtBr). The aggregation of the 1:1 complex units through $\pi\cdots\pi$ interactions developed during a period of time could result in the growth of the species in the solution. This has been further supported by adding EtBr that prevents such aggregation since EtBr is expected to show strong $\pi\cdots\pi$ interactions. Addition of EtBr indeed arrested the fluorescence enhancement that was otherwise observed in the solution without the presence of this. Thus the prevention of aggregation of the complex units in the presence of EtBr has been shown in case of [L+Phe] in comparison with the corresponding control as shown in Figure 4.

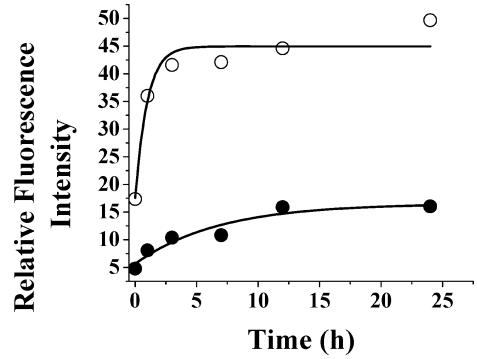

Figure 4. Relative fluorescence intensity as a function of time for 1:2 solutions of L and Phe. The filled ones are in the presence of 5 equiv of EtBr and the unfilled ones are the corresponding control without the EtBr.

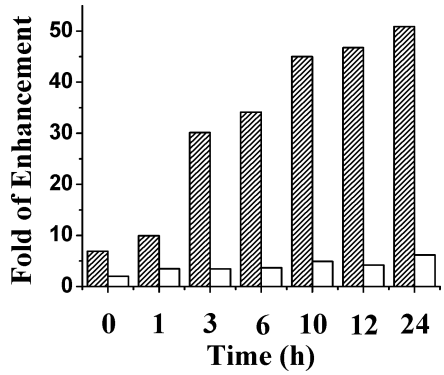

Figure 5. Histogram showing the fold of fluorescence enhancement for the titration of L *vs* Phe in the absence (dashed) and in the presence (blank) of 9-anthracenaldehyde.

Prevention of Aggregation in the Presence of 9-Anthracenealdehyde (9-AA). The role of aromatic moiety in the disruption of the fiber formation has been further addressed by carrying out two types of fluorescence experiments using 9-anthracenealdehyde (9-AA). In one experiment, the 9-AA was added to a mixture of L and Phe at the beginning, and the fluorescence spectra were measured as a function of time. In the presence of 9-AA, no significant increase was observed in fluorescence intensity, while in the control experiment performed without the addition of 9-AA, it exhibited an increase in the fluorescence by ~50 fold, indicating the fiber formation is prevented in the presence of 9-AA (Figure 5). In another experiment, the fibers were initially allowed to form by mixing L and Phe and leaving the solution for 24 h before 9-AA was added in different mole ratios. A progressive quenching of the fluorescence was observed, suggesting the disruption of the fibers formed (SI 03).

Microscopy Studies. Since the initially formed [L+Phe] complex aggregates as a function of time through the $\pi\cdots\pi$ interactions extended between these complex units, the resulting oligomeric/polymeric and/or fiber species was explored based on atomic force microscopy (AFM), transmission electron microscopy (TEM), and scanning electron microscopy (SEM), as a function of time after the addition of Phe to L. The results have been compared with the data obtained for the control molecular systems.

AFM Studies. The AFM studies were carried out to assess the formation of fibers between L and Phe, as well as other aromatic side chain amino acids (Trp and Tyr) and also those not possessing such a side chain (Ala, Pro). The fiber formation has also been studied with different controls for appropriate comparison.

In the Presence of Phe. In AFM, the micrographs have been measured for the samples drawn at different time intervals after the addition of Phe to L (Experimental Section). Immediately after the addition of both the components (at time zero), discrete particles of spherical shape were observed with no indication of fiber formation (Figure 6a,b). Within 4 h, these spherical particles started to merge together to form micelles and/or vesicular morphology with a dumbbell shape (Figure 6c,d). Such self-assembled morphology could generate short fibers over a period of time. After 8 h, the formation of the fibers could be clearly seen, and these were well spread all over the mica surface (Figure 6e,f). Though most of the fibers are parallel to each other, some branched chain fibers were also observed. Careful examination of these long fibers formed from the samples prepared at lower concentration revealed that these were actually made up of shorter ones (Figure 6g,h). The shorter ones have lengths of 450−530 nm,

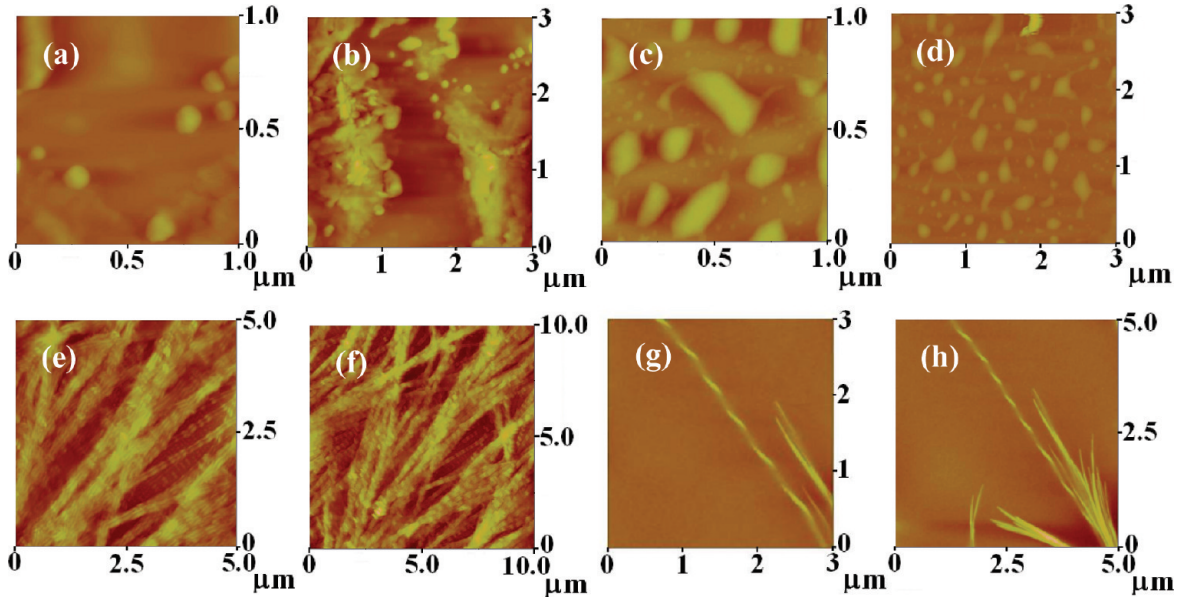

Figure 6. AFM micrographs of [L+Phe] where the samples were drawn at different time intervals: (a and b) immediately after mixing; (c and d) after 4 h; (e and f) after 8 h, and (g and h) after 8 h but with the samples from an experiment carried out using lower concentration.

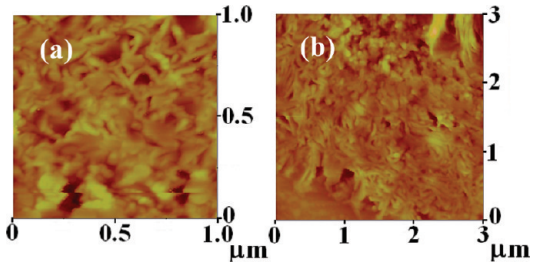

Figure 7. AFM micrographs of [L+Phe] where the sample was drawn after 24 h. Panels a and b are from different regions of the sample on mica.

widths of 90−160 nm, and heights of 13−18 nm. It can be noted that the width of the fiber is much higher as compared to their height, imparting a ribbon-like structure to the fiber[36] through the bundling of a number of individual threads in a parallelepiped fashion. These dimensions seem to fit well with the stacking of about 250−300 complex units along the length and stacking of 20−30 such fibers bundled in the width of the ribbon. The undulation morphology of the fibers observed can be the result of the structural defects formed during the process of $\pi \cdots \pi$ stacking.[3]

After 24 h, the long fibers of [L+Phe] were no more observed, instead, a high population of smaller fibers were noticed in the micrographs of AFM as shown in Figure 7, as the shorter ones may have resulted from the breakage of the sufficiently long fibers on the surface of the mica.

In the Presence of Trp and Tyr. Since Trp and Tyr possess aromatic side chains, the fibers formed by these were studied by AFM. In the case of [L+Trp], the initially formed spherical particles were joined together to form dumbbell-shaped particles in about 4 h. The fibers formed by Trp after 24 h were short and clustered, and the abundance of fiber formation is rather low when compared to [L+Phe] (Figure 8a,b). On the other hand, the fibers formed from [L+Tyr] were branched but not well spread as that observed in case of [L+Phe] (Figure 8c,d).

In the Presence of Ala and Pro. However, in case of [L+Ala], the initially formed spherical particles (sizes of 39−80 nm and heights of 2−4 nm) continue to grow in size but maintain a spherical shape, where the sizes of the particles (sizes of 156−314 nm and heights of 5−11 nm) are about 4−8 times greater than the initial particles when measured after 8 and 24 h (Figure 9a,b). Even proline does not show any fibers after 24 h (Figure 9c,d). Thus no fibers were found in the case of [L+Ala] and [L+Pro] even after 1 day, suggesting that the presence of the phenyl side chain is essential for the amino acid amphiphile to form fibers with the amphiphile L.

In the Presence of 3-PPA. In case of [L+3-PPA], the initially formed spherical particles (sizes of 20−90 nm and heights of 5−14 nm, Figure 10a) continue to grow in size but maintain a spherical shape, where the sizes of the particles (sizes of 180−260 nm and heights of 17−25 nm, Figure 10b) is about 10 to 14 times higher than the initial sizes when measured after 8 h. Over a period of 24 h, these particles tend to aggregate to form bigger ones with no well-defined shape (Figure 10c). Thus no fibers were found in the case of [L+3-PPA] even after 1 day since an initial complex between L and 3-PPA was not formed. Nonformation of the initial complex between L and 3-PPA has already been demonstrated by fluorescence titration studies. All these results further suggest that the presence of phenyl side chain moiety is essential for the amino acid to form fibers with L.

In the Presence of NaCl and $Zn(ClO_4)_2$ Salt. The role of hydrogen bonding and hydrophobic interactions in the formation of the fibers has been further studied by judging the fiber formation or its disruption under the presence of these salts. AFM experiments were carried out using two different salts, NaCl and $Zn(ClO_4)_2$, owing to their diverse interactions in coordination chemistry. From each of the metal salts, two experiments were carried out. (a) One was carried out by adding the salt to the [L+Phe] mixture initially followed by measuring AFM after 12 h, and it was found that none of these salts allow the fiber formation (Figure 11). (b) The other was carried out by adding the salt after the fibers were formed, and disruption of the fibers was found with both the salts. Thus, these salts do not allow fiber formation and were capable of breaking the fibers, if already formed.

AFM Studies with Galactosyl-salicyl-imino Conjugate (L_1) and Phe. To find out whether the fibers formed are dependent on the glycose part of the glyco-conjugate, AFM studies were carried out between an analogue of L, galactosyl-salicyl-imino conjugate (L_1),[34] and Phe. No

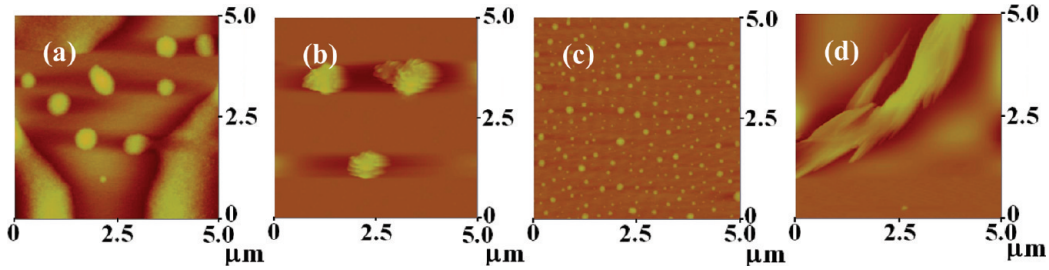

Figure 8. AFM micrographs of the samples drawn from [L+Trp] in the case of (a and b) and from [L+Tyr] in case of (c and d). Among these the first one is at 0 and the second one is at 24 h.

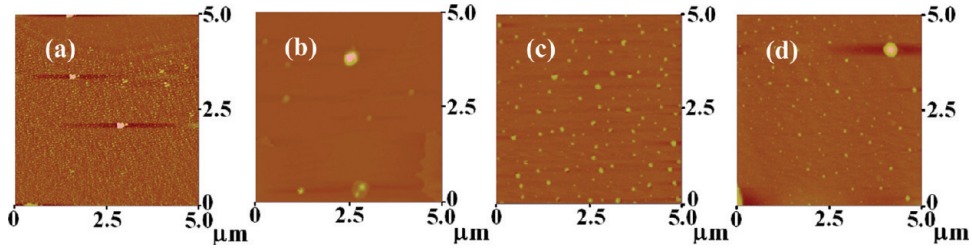

Figure 9. AFM micrographs of the samples drawn from (a and b) [L+Ala] and from (c and d) [L+Pro]. Among these the first one is at 0 and the second one is at 24 h.

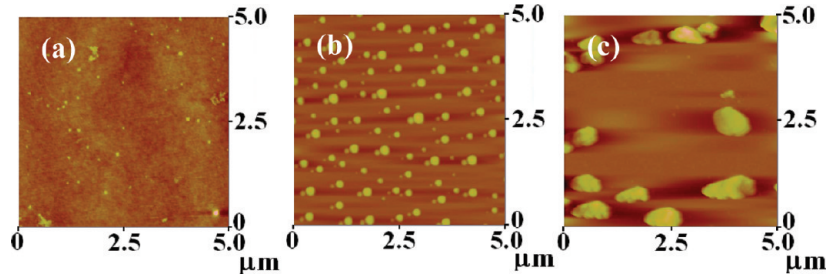

Figure 10. AFM micrographs of [L+3-PPA] samples drawn at different time intervals: (a) immediately after mixing; (b) after 8 h, and (c) after 24 h.

formation of fibers was found suggesting that the growth of the fibers is dependent on the nature of the glycose part (Figure 12).

The precursor molecules, L or Phe, alone do not show the formation of fibers of the nature demonstrated for [L+Phe] when left in solution even over a period of 1 day as studied based on AFM (Supporting Information, SI 04). Based on the AFM studies, it is possible to arrange these in the order of their fiber formation ability: Pro and Ala (no fibers) $\ll$ Trp (short bundles and less abundant) $<$ Tyr (thin, branched, bundled and less abundant) $<$ Phe (best fiber formation and growth and high abundance).

TEM Studies. TEM micrographs measured after 8 h of mixing of L with Phe reveal the fibrous nature of the species. The lengths of the fibers were found to be in the range of 100−200 nm, and the widths were 10−20 nm (Figure 13a,b). In both the AFM and TEM studies, the fibers were found to be more aggregated. This may be due to the enhanced interfiber interactions as a result of less efficient packing among the molecules within the individual nanofibers. Even the micrographs measured by high resolution TEM exhibit bunches of fibers as can be seen from Figure 13c,d. Some peptide amphiphiles conjugated with polydiacetylene also formed such fibers upon photoirradiation as reported in the literature.[3]

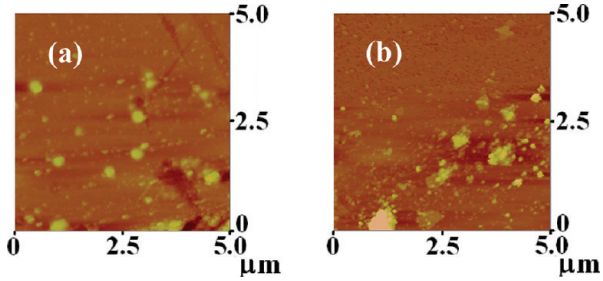

Figure 11. AFM micrographs of [L+Phe] obtained in the presence of (a) NaCl and (b) $Zn(ClO_4)_2$ after 12 h.

SEM Studies. Scanning electron micrographs obtained for the powder isolated from the immediately prepared reaction mixture of L and Phe exhibited large crystallites of the size 10−15 μm × 2−3 μm (Figure 14a). The powder isolated after 8 h of reaction, exhibited branched fibers (Figure 14b). The micrograph measured from the powder obtained from the reaction mixture of L and Phe after 24 h exhibited rodlike fibers (Figure 14c). SEM images of the precursor L exhibit very long crystalline rods (Supporting Information, SI 05).

Samples of [L+Ala] and [L+3-PPA] obtained even after 24 h exhibited no fibers unlike that observed in the case of [L+Phe], supporting that the side chain phenyl moiety is absolutely essential for the formation of the fibers (Figure 15).

Though all the three microscopy studies exhibited fiber formation, there seemed to be some basic differences in their size parameters owing to the surfaces used, namely, mica in case of AFM and carbon-coated copper grid in the case of TEM. Further differences may arise from the desolvation technique used, namely, high vacuum for TEM and simple air drying in the case of AFM.

Powder XRD Studies. Powder XRD studies were carried out with the solid samples obtained from the reaction mixture of [L+Phe] at different time intervals (Experimental Section). The diffractograms shown in Figure 16 are clearly characteristic of crystalline material and exhibit appreciable variation in the intensity and/or breadth of some peaks when compared to the unaltered ones, where the experiments were carried out on the samples drawn at different time intervals. Compari-

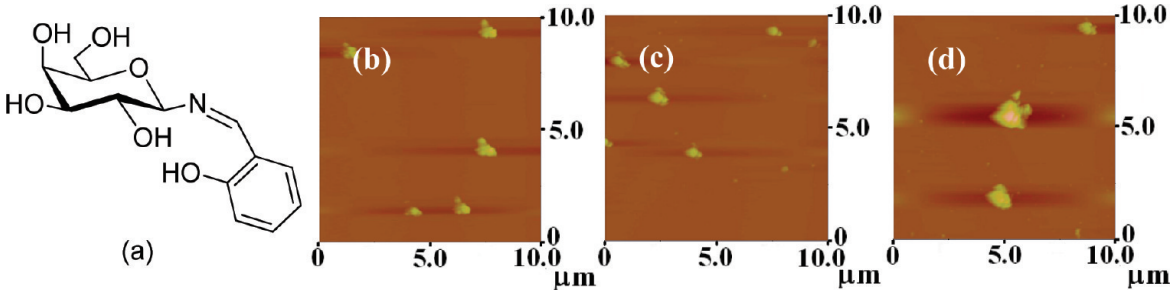

Figure 12. (a) Schematic structure of galactosyl-salicyl-imino conjugate (L_1). AFM micrographs of the samples drawn from [L_1+Phe] at different time intervals: (b) 0 h, (c) 8 h, and (d) 24 h.

son of these diffractograms revealed increased peak intensities with those observed at 2θ values of 13.80, 17.36, 19.23, and 20.73 and a decreased peak intensity at a 2θ value of 40.20. In some cases the peaks were merged or sharpened (2θ = 26.92, 32.86). These lines could not be indexed in the absence of any reference compound. Thus the powder XRD studies provided qualitative information on the crystallinity of the nanofibers formed in the case of L and Phe, as also noticed from SEM studies.

DLS studies. To test the feasibility of the fiber formation as noticed based on microscopy, DLS studies (Supporting Information, SI 06) were carried out as a function of time. It is expected that the solvo-dynamic diameter of the self-assembled species increases over a period of time. Hence the solutions were scanned at different time intervals for DLS, and the results are shown in Figure 17. Appropriate control studies have also been performed with simple glucosyl-salicyl-imine-conjugate amphiphile (L) as well as with phenylalanine. As can be seen from Figure 17, the peaks of the self-assembled species were shifted to a higher diameter range with increase in time (Supporting Information, SI 06). At zero time, the mean diameter of the species was found to be in the range of ~0.12 μm which gradually increases to ~6.5 μm after 18 h. The progressive increase observed in the solvo-dynamic diameters of the species can be attributed to the formation of different kinds of self-assembled ones. The small diameter species observed at the beginning may result from 1:1 complex by forming a cluster. Observation of peaks with larger diameter (after 4 h) supports the formation of the nanofibers that takes some time to grow as it is a slow kinetic process. L alone or phenylalanine alone ex-

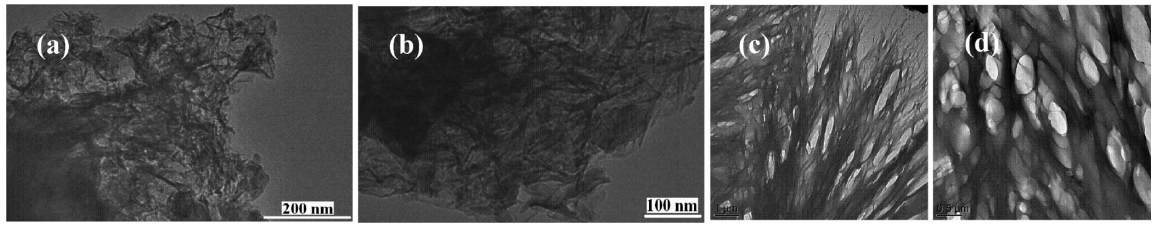

Figure 13. TEM micrographs of the sample drawn from [L+Phe] mixture after 8 h: (a and b) normal TEM and (c and d) high-resolution TEM.

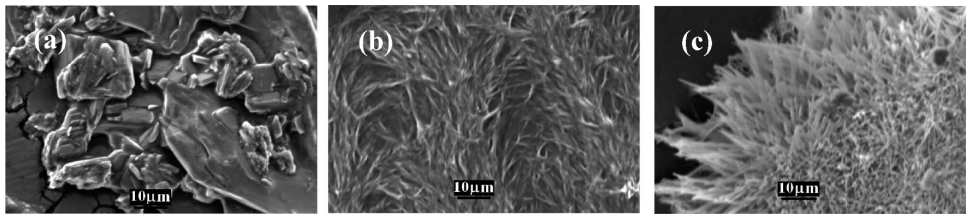

Figure 14. SEM micrographs of the sample drawn from [L+Phe] mixture at different time interval: (a) immediately after mixing, (b) after 8 h, and (c) after 24 h.

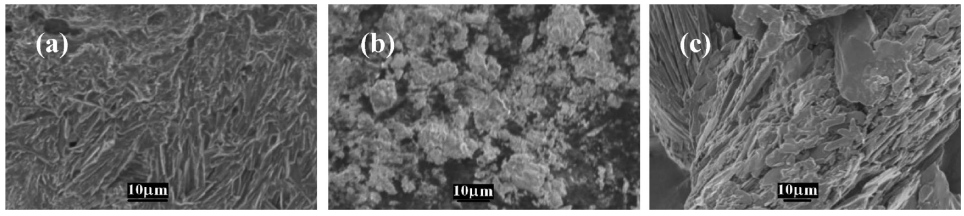

Figure 15. SEM micrographs of the sample drawn from the experiments carried out with control molecular systems: (a) [L+Ala] after 8 h, (b) [L+Ala] after 24 h, (c) [L+3-PPA] after 24 h.

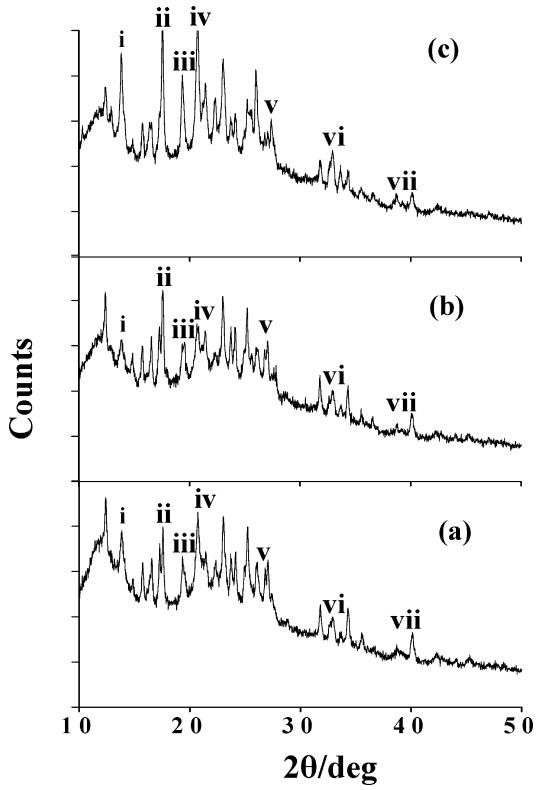

Figure 16. Powder XRD diffractograms of [L+Phe] where the samples were drawn at (a) 0 h, (b) 8 h, and (c) 24 h. The peaks of interest are indicated by roman marking.

hibited no considerable aggregation in solution even after one day (Supporting Information, SI 06).

Computational Modeling of Nanofibers. From the spectroscopic and microscopy studies, it has been shown that the complex unit formed between L and Phe grows further over a period of time to result in the formation of nanofibers. To model the formation of the fiber, molecular-mechanics-based computational calculations were carried out using HYPERCHEM (Experimental Section).[37] The fiber was modeled by replicating the 1:1 complex unit structure obtained from the DFT computations[38] (Supporting Information, SI 07a) in a cascade manner by forming its oligomers possessing 2, 4, 8, 16, and 32 units. The modeled oligomers were then minimized using different force fields, namely, MM+, BIO+(CHARMM), and Amber, and it was found that the MM+ based calculations yielded better results when compared to the others. The dimeric structure was obtained by minimizing the two individual 1:1 complex units placed apart. Similarly, a tetrameric structure was obtained by minimizing two dimers placed at a noninteracting distance. This procedure was continued until a 32-unit thread was formed. Formation of such a thread is unidirectional with dimensions of (0.60 ± 0.05) × (0.90 ± 0.05) × (38.0 ± 0.2) nm^3 (Figure 18). However, the attempts to form the 1:1 complex of L and the control molecular system 3-PPA were futile, indicating that there is no complex formed between L and 3-PPA (Supporting Information, SI 07b). Indeed we found the same from the fluorescence titration studies. A closer examination of the threads of [L+Phe] exhibited π···π interactions (phenyl···phenyl distance being ~3.9 ± 0.1 Å) of the type ...ABABABAB....

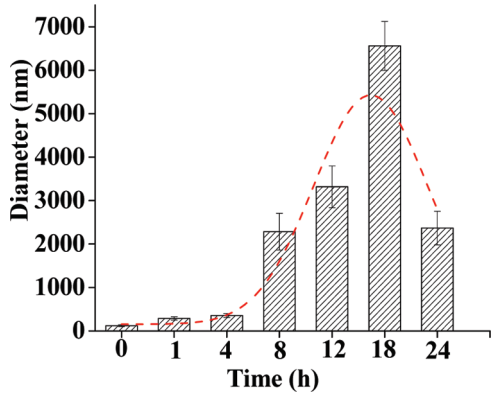

Figure 17. Particle size distribution plot of the species formed at different time interval by dynamic light scattering (DLS).

On the other hand, when the side chain of the amino acid was replaced by methyl moiety to mimic alanine in place of the phenylalanine in the threads, the corresponding thread was broken into smaller pieces with no long-range order, suggesting that the fiber formation is not favored when there is no phenyl side chain (Figure 19).

To see whether L alone forms any polymeric thread through π···π interactions, MM+ minimizations were performed by taking a 16-unit thread of [L+Phe] followed by removing the Phe units from the same. This resulted in the breakage of the thread to form at least six smaller aggregates of L. Among these, only two aggregates exhibited π···π interactions and not the others (Supporting Information, SI 07c). Thus the MM+ study suggests that L alone does not form a thread without the presence of Phe and hence supports the experimentally observed results.

Comparison of the cross-sectional dimensions of the thread built on the basis of the computational study with that observed from microscopy suggests that several threads must have been bundled together to form the fibers. The bundling of the individual threads to result in the fibers was achieved by carrying out MM+ minimization on 16 threads. This minimization was carried out by a cascade process by initially making a bundle of 2 followed by 4 followed by 8 and then followed by 16, sequentially at every stage and using the output at each stage for the next higher one. To keep the computational times low, the bundling of the threads to form a fiber was made using threads of 16 unit length rather than that of the 32, as shown in Figure 20. The minimized bundle exhibited dimensions (2.5 ± 0.02) × (4.0 ± 0.03) × (16.9 ± 0.3) nm^3. Similar computations carried out with Tyr resulted in a polymer that has several nucleating sites for branching (Supporting Information, SI07).

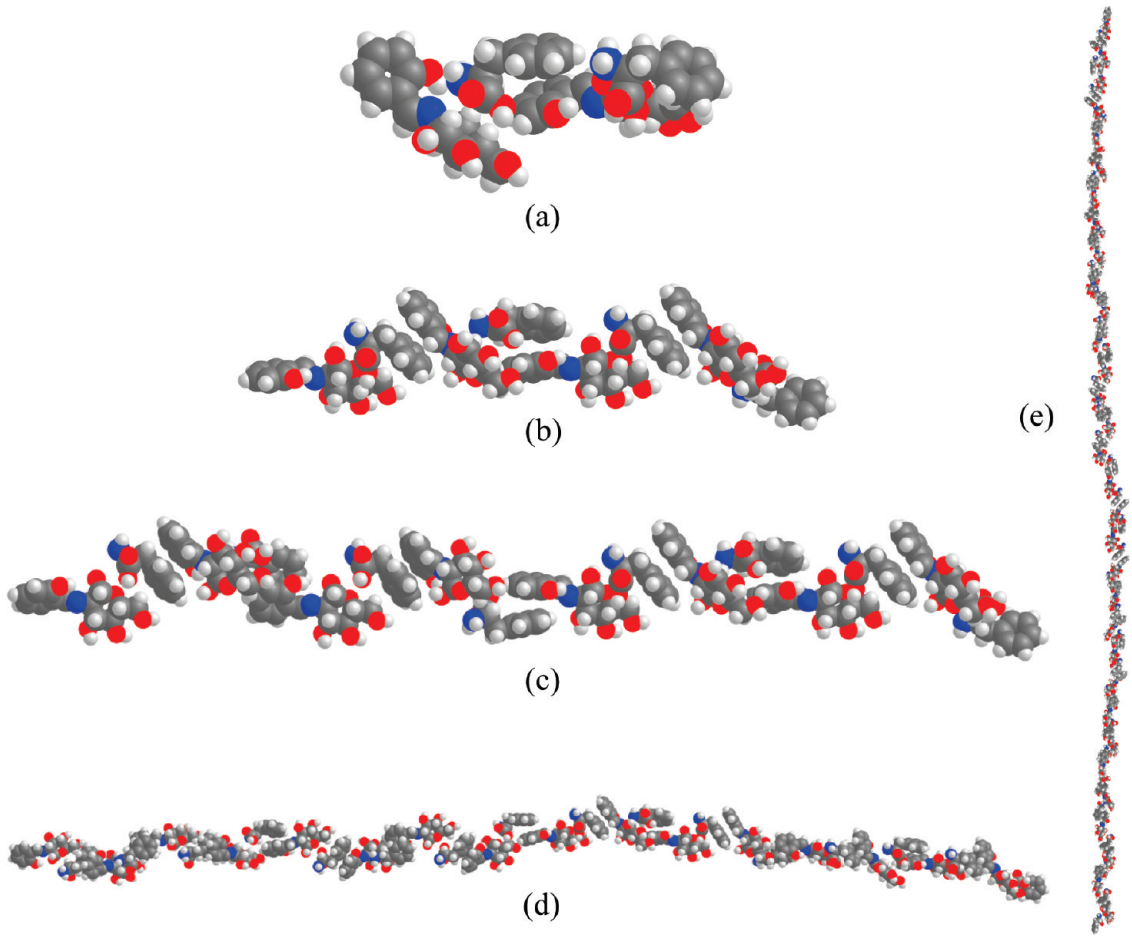

Figure 18. Minimized structures obtained from the MM+ calculations performed using a 1:1 complex of L and Phe: (a) 2-mer; (b) 4-mer; (c) 8-mer; (d) 16-mer; and (e) 32-mer.

Protein—Fiber Interactions. In view of the importance of the biocompatible nanofibers in medical applications, such as tissue engineering and drug delivery, the nanofibers formed from L and Phe as reported in this paper were studied for their interaction with different serum and legume proteins. While the serum proteins used were highly α-helical in nature, the legume proteins used were highly β-sheet in nature.

The fiber-forming reaction mixture was initially prepared in the presence of the corresponding protein, and the formation of the fiber and the characteristics of the protein were monitored by atomic force microscopy. All the three albumin proteins studied, BSA, HSA, and lactalbumin, allow the formation of fibers, as can be seen from the AFM images (Figure 21, Supporting Information, SI 08). From the micrographs, it is further evident that the branching nature of the fibers is mostly unaltered in the presence of either BSA or lactalbumin, but the branching is almost diminished in the presence of HSA. While these fibers were found to be noninterac-

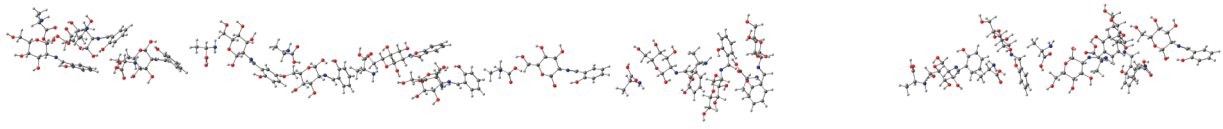

Figure 19. MM+ minimization results obtained of a 16-mer fiber of (L+Phe) where the Phe was replaced by simple Ala, leading to smaller fragments.

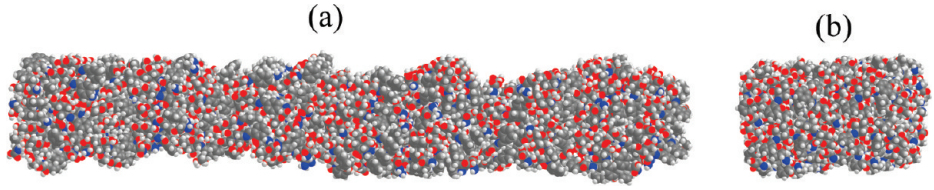

Figure 20. Bundle of fiber obtained from molecular-mechanics-based minimization of 16 threads of a 16-mer [L+Phe]: (a) view along the length and (b) a cross-sectional view.

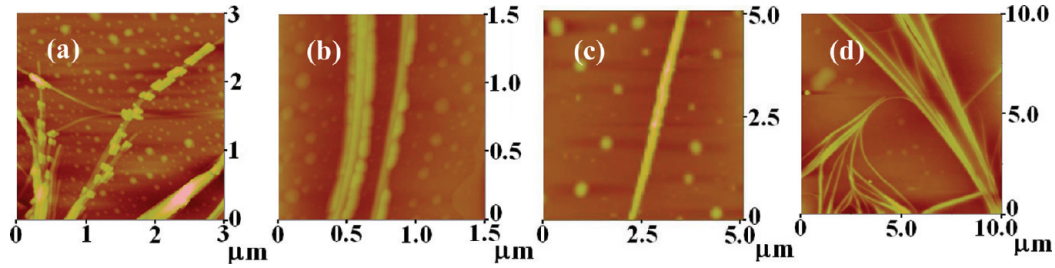

Figure 21. AFM micrographs of (a, b) {[L+Phe]+BSA}, (c) {[L+Phe]+HSA}, and (d) {[L+Phe]+lactalbumin} samples.

tive in the case of HSA and lactalbumin, the BSA protein molecules were indeed found to adhere to the fibers. A closer examination of the AFM features reveal that while simple BSA protein exhibits spherical particles, the same when bound to the fibers resulted in deformation and hence nonspherical particles, which may be attributed to the conformational and/or shape changes occurring in the BSA. Such deformations have been observed, as reported in the literature, when large proteins and/or other macromolecules were adsorbed/bound to solid materials.[39] In the present case, the deformation of the BSA particles may have allowed the protein to unfold to some extent, which in turn exposes additional sites that would involve in interaction with the fibers. However, for the β-sheet proteins, namely, peanut agglutinin and jacalin, no such fiber formation was observed suggesting that these proteins inhibit the formation of fibers (Figure 22). Thus among the five proteins belonging to the two different classes studied and reported in the paper, only BSA selectively adheres, and hence these fibers would be of interest in a variety of applications.

Circular Dichroism (CD) Studies. To understand the changes that may occur in the secondary structures of these proteins when they interact with the fiber, CD titrations were carried out. Appropriate control experiments were performed and subtracted before interpreting the observed results. During the titration, the protein concentration was kept constant by adding varying amounts of fiber forming mixture (Experimental Section). The CD spectra shown in Figure 23a for the titration with BSA shows considerable change in the secondary structural features by strengthening the helicity of the protein owing to the possible interactions present between the fiber and the protein, though one may expect to disrupt the secondary structures upon interaction of protein with the fiber. Increase in the negative ellipticity has also been observed with small peptides, over a period of time, forming nanofibers.[40] On the other hand, the HSA which does not adhere to the fiber but only allows the fiber to form, seems to bring only marginal changes in the ellipticity (Figure 23b) as studied by CD in solution. The slope of ellipticity *versus* concentration is at least one-half in the case of HSA when compared to that of BSA. Similar titrations carried out with β-sheet proteins, such as jacalin, Figure 23c, exhibited no significant changes in the ellipticity, and these result are in line with that observed from the microscopy, namely, no fiber formation (Supporting Information, SI 09).

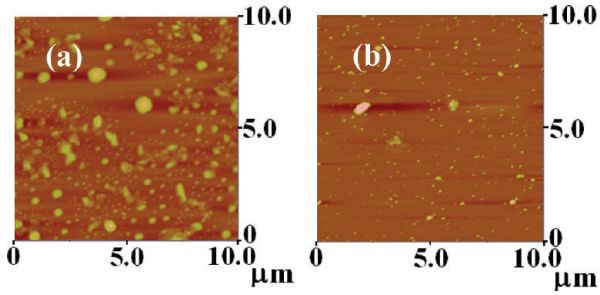

Figure 22. AFM micrographs of (a) {[L+Phe]+PNA} and (b) {[L+Phe]+jacalin} samples.

CONCLUSIONS AND CORRELATIONS

Molecular self-assembly of biocompatible systems is an interesting target in current research due to its applications in materials as well as in clinical sciences. The self-assembly process among amphiphiles is governed by several noncovalent interactions. Though the individual effect of these interactions are minimal as far as the energetics are concerned, when acting together, they can generate well-ordered supramolecular structures. Among the various noncovalent interactions responsible for such self-assembly, $\pi\cdots\pi$ interactions play an important role. Herein, we report the self-assembly of two different amphiphiles, a glucosyl-salicyl-imino-conjugate (L) and a phenylalanine, forming nanofibers over a period of time through $\pi\cdots\pi$ interactions.

A progressive increase in the fluorescence intensity has been observed as a function of time with phenylalanine. Simple amino acids, such as glycine and alanine, as well as the simple carboxylic equivalent of phenylalanine, 3-phenylpropionic acid (3-PPA), do not show significant changes in the fluorescence intensity, suggesting that both the amino acid portion as well as the side chain phenyl moiety together are needed in the same molecule to show these changes. The fluorescence and absorption spectral changes observed in the titration of L with Phe are consistent with the formation of an initial 1:1 complex followed by aggregation of these. Though the observations in the case of glycine and alanine indicated the initial formation of a 1:1 complex, there is no indication for their further aggregation even

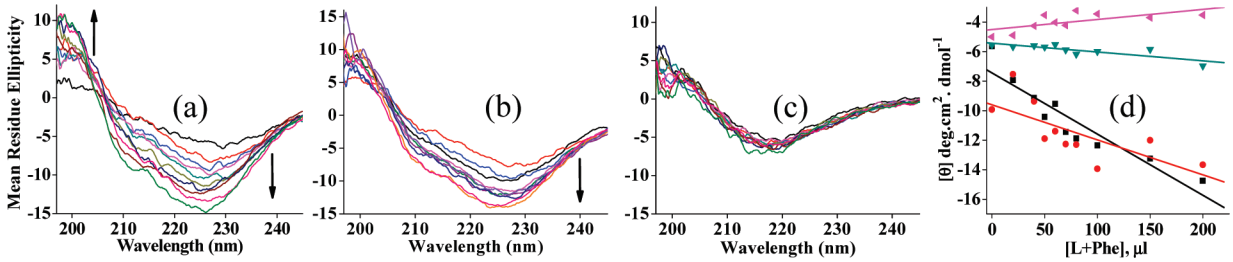

Figure 23. Plots of mean residue ellipticity as a function of volume of [L+Phe] addition in the case of: (a) {[L+Phe]+BSA}, (b) {[L+Phe]+HSA}, and (c) {[L+Phe]+Jacalin}. (d) Plots of ellipticity as a function of volume of [L+Phe] addition in case of proteins and lectins: (black) BSA, (red) HSA, (green) Jacalin, and (pink) PNA.

over a period of 1 day. However, under similar experimental conditions, the observations with 3-PPA does not conform either to the formation of 1:1 complex or to its aggregation. The aggregational behavior observed with phenylalanine has been further established by MALDI where the higher aggregate peaks were observed over a period of time. Formation of such aggregates has been indirectly shown by preventing the same using ethidiumbromide.

AFM, TEM, and SEM studies clearly revealed the formation of nanofibers as a function of time after mixing L with phenylalanine. The length and breadth (in nm) of the individual fibers was found in the range of 450−530 and 90−160 and 100−200 and 10−20, respectively, from AFM and TEM. Similar microscopy studies carried out between L and alanine or 3-phenylpropionic acid did not show any fiber formation. Though some fiber formation was observed in case of Trp and Tyr, the nature and abundance of the fibers formed greatly differs from those formed from Phe. Even the change in the carbohydrate moiety, such as changing from glucosyl to galactosyl, does not result in the formation of nanofibers, suggesting the role of glycomoiety in the formation of these fibers. The growth of the fibers as a function of time in the case of [L+Phe] has also been supported by DLS experiments. These fibers were found to be crystalline on the basis of powder XRD studies.

Computational modeling of the nanofiber formation was carried out by taking the DFT optimized 1:1 complex and building the fiber by going through a cascade methodology using molecular mechanics, wherein a dimer is being made from a single complex unit, and a tetramer from two such dimers, and an octamer from two such tetramers, and so on. The modeling clearly revealed a $\pi\cdots\pi$ interaction of the phenyl moiety of phenylalanine with the phenyl moiety of the L resulting in ...ABABAB...-type of arrangement. A 32-unit thread exhibit dimensions of (0.60 ± 0.05) × (0.90 ± 0.05) × (38.0 ± 0.2) nm^3. However, when the Phe is being replaced by Ala that lacks side-chain phenyl moiety, the initial thread of [L+Phe] was broken to give smaller fragments. Even L alone does not show the formation of the threads. To model the widths noticed in the microscopy, computational studies were carried out to give bundles of these threads using molecular mechanics calculations. A bundle formed from 16 threads of a 16-mer exhibited dimensions, (2.5 ± 0.02) × (4.0 ± 0.03) × (16.9 ± 0.3) nm^3.

Because of the biocompatibility of these amphiphiles, their self-assembled nanofibers can probably be used as a new class of molecular transporters or as a protective coating agent over the drugs for delivery. The AFM studies carried out to test the applicability of these fibers resulted in the observation that only BSA selectively adheres among the five proteins belonging to two different classes reported in the paper. The changes occurred in the secondary structural features of these proteins in fiber-forming solutions were studied by CD spectroscopy. Hence these fibers would be of interest in the recovery of BSA from a mixture of proteins and/or transfer of a chemical entity/drug between the fibers and BSA selectively. Suitable biocompatible fibers in the literature have indeed been used for making biodegradable bandages for wounds.[39]

EXPERIMENTAL SECTION

For all the studies reported in this paper, the D-stereoisomer of glyco-conjugates and the L-stereoisomer of amino acids have been used.

Characterization of L. Glucosamine hydrochloride (0.215 g, 1 mmol) salt was neutralized with triethylamine in ethanol before being used in the synthesis. To this, salicylaldehyde (0.15 mL; 1 mmol) was added. The reaction mixture was refluxed for 6 h at 60 °C. The solid product formed, L, (0.25 g) was filtered and washed with cold ethanol several times followed by diethyl ether and was dried under vacuum. Yield −87%. ^{1}H NMR (DMSO, δ ppm): δ 2.5 (q, 6H, DMSO), 3.25−3.80 (m, 5H, carbohydrate skeletal C−H), 4.53−4.95 (4d, 4H, C1-OH, C3-OH, C4-OH, C6-OH), 5.16−5.18 (d, H, J-5.5 Hz), 6.19−7.59 (2d, 2t, 4H), 8.6 (s, 1H, CH=N), 13.2 (s, 1H, Ar−OH) ppm. Anal. Calcd for $C_{13}H_{17}NO_6$: C, 55.12; H, 6.05; N, 4.94. Found: C, 54.85; H, 6.61; N. 4.86 ESI-MS *m/z* 284 ($[M+H]^+$, 100%).

Fluorescence and Absorption Studies. Fluorescence emission spectra were measured on Perkin-Elmer LS55 fluorescence spectrophotometer by exciting the samples at 320 nm, and the emission spectra were recorded in the 330−550 nm range. Absorption studies were carried out with a JASCO V-570 instrument by measuring the spectra from 800 to 200 nm. The bulk solutions of L and amino acids were prepared in methanol in which 400 μL (4%) of water was added for initially dissolving the amino acid. The bulk solution concentrations were maintained at 1 × 10^{-3} M. All the measurements

were made in 1 cm quartz cell, and the effective concentration of L was maintained as 50 μM. During the titration different mole ratios of amino acid were added to L, and the emissions of all the samples were measured at different time intervals. In the case of the phenylalanine titration, the background spectra were subtracted.

For the EtBr experiment, the bulk solutions of L, amino acid, and EtBr were prepared in methanol. The bulk solution concentrations were maintained at 1×10^{-3} M. During the titration, initially L and EtBr were mixed in 1:2 mol ratio by fixing the effective concentration of L at 50 μM. Different mole ratios of amino acids were added to these solutions, and all the emission measurements were made at different time intervals.

For the fluorescence experiment with 9-anthracenaldehyde, 150 μL of L (50 μM) was added to 300 μL of 9-anthracenaldehyde (2 equiv) and mixed initially, followed by the addition of increasing amount of Phe (0, 75, 150, 300, 450, 600 μL).

MALDI TOF Studies. Mass spectra were collected using an Axima-CFR MALDI-TOF-MS (Kratos Analytical, Manchester, UK), in the positive ion mode. The concentrations of the samples were kept the same as in the case of the solution studies.

Microscopy Studies. AFM studies were performed in multimode Veeco Dimensions 3100 SPM with Nanoscope IV controller instrument. Tapping mode with a phosphorus-doped Si probe having a sharp fine tip at the end was used in all the cases. TEM experiments were performed with a PHILIPS CM200 transmission electron microscope operating at 20−200 kV (resolution, 2.4 Å). High resolution TEM was done on a JEOL JEM 2100F instrument. Carbon-coated copper grids of 400 mesh were used as substrate for the sample. SEM studies were carried out with JEOL JSM-6390 scanning electron microscope. Powder XRD studies were performed with a PHILLIPS PANalytical X-Pert Pro diffractometer. The solvo-dynamic diameter of all the samples were measured in methanol (concentration were kept the same as in the case of fluorescence studies) at 25 °C. The incident laser (Coherent Inc., Santa Clara, CA) radiation used was a 633 nm wavelength of 90°. The scattered light was filtered through a vertical polarization filter. The experiments were carried out using standard cylindrical BI-RC 12 glass cuvettes.

Sample Preparation. For AFM, TEM, and DLS studies, L and Phe solutions were made in methanol. Phe solutions were made by dissolving the amino acids in ~400 μL of deionized water and then adding methanol to the desired volume. The bulk concentration of the solutions was *ca.* 1×10^{-3} M for all the cases. For studies at lower concentration, the bulk concentration of L and Phe was *ca.* 1×10^{-4} M. For AFM studies with proteins, 100 μL of protein (1 mg/10 mL) was added to 100 μL of [L+Phe]. For the AFM studies of [L+Phe] in the presence of salts, the bulk concentration of NaCl and $Zn(ClO_4)_2$ was *ca.* 1×10^{-3} M.

For AFM and TEM studies, 1.0 mL of L and 1.0 mL of Phe was added to a sample vial, and this mixture was used as stock solution. For DLS studies, 100 μL of L and 100 μL of Phe were added to 3.0 mL of methanol solution. Different sample vials were prepared for drawing the samples at different times, and the concentration of these samples was maintained throughout.

For AFM, an aliquot of ~200 μL was taken from the stock solution at different time intervals and sonicated for ~15 min. Different sample blocks were prepared by spreading ~50 μL of the mixed solution on a mica sheet and allowing the prepared sheet to dry in air at room temperature. For TEM, the same procedure was followed, and the mixed solution was spread over a carbon-coated copper grid which was then allowed to air-dry.

For powder XRD and SEM studies the solid samples were isolated from the mixture of [L+Phe] at different time intervals and used for experiments.

Computational Studies. Coordinates of 1:1 complexes of [L+Phe] was taken from the DFT calculations and were used as templates for the construction of dimers and higher order oligomers. The dimer was constructed initially by taking two 1:1 complex units and placing them farther apart and then minimizing the same. A tetrameric unit was built from two dimers and was minimized. This procedure was adopted to generate higher oligomeric units, namely, 8, 16, and 32. The threads were minimized at each stage before going for the higher aggregate. Hence all the calculations were performed on the MM+ force field. Such minimized threads were taken to form a bundle and were minimized through molecular mechanics calculations.

CD Studies. CD studies were performed with a JASCO J-815 circular dichroism spectrometer. For CD studies with proteins, the protein concentration was kept constant. Hence 40 μL of protein (1 mg/mL) was added to varying concentrations of [L+Phe], and the spectra were recorded.

Acknowledgment. This paper is dedicated to Professor Stephen J. Lippard of Massachusetts Institute of Technology on the occasion of his 70th birthday. C.P.R. acknowledges the financial support from DST, CSIR, and DAE-BRNS. A.A. and A.M. acknowledge CSIR for SRF. We thank IIT Bombay for AFM (DST-FIST, Department of Physics), TEM and HR-TEM (SAIF), SEM (Earth Sciences Department), powder XRD (Department of Physics), and DLS (CRNTS).

Supporting Information Available: Characterization and spectral data of L (SI 01); fluorescence data (SI 02); absorption data (SI 03); AFM data (SI 04); SEM data (SI 05); DLS data (SI 06); computational data (SI 07); AFM studies with proteins (SI 08); and CD studies with proteins (SI 09). This material is available free of charge *via* the Internet at http://pubs.acs.org.

REFERENCES AND NOTES

1. Whitesides, G. M.; Mathias, J. P.; Seto, C. T. Molecular Self-Assembly and Nanochemistry: A Chemical Strategy for the Synthesis of Nanostructures. *Science* **1991**, *254*, 1312–1319.
2. Lehn, J. M. Supramolecular Chemistry. *Science* **1993**, *260*, 1762–1763.
3. Hsu, L.; Cvetanovich, G. L.; Stupp, S. I. Peptide Amphiphile Nanofibers with Conjugated Polydiacetylene Backbones in Their Core. *J. Am. Chem. Soc.* **2008**, *130*, 3892–3899.
4. Pakalns, T.; Haverstick, K. L.; Fields, G. B.; McCarthy, J. B.; Mooradian, D. L.; Tirrell, M. Cellular Recognition of Synthetic Peptide Amphiphiles in Self-Assembled Monolayer Films. *Biomaterials* **1999**, *20*, 2265–2279.
5. Berndt, P.; Fields, G. B.; Tirrell, M. Synthetic Lipidation of Peptides and Amino Acids: Monolayer Structure and Properties. *J. Am. Chem. Soc.* **1995**, *117*, 9515–9522.
6. Yu, Y.-C.; Berndt, P.; Tirrell, M.; Fields, G. B. Self-Assembling Amphiphiles for Construction of Protein Molecular Architecture. *J. Am. Chem. Soc.* **1996**, *118*, 12515–12520.
7. Murakami, Y.; Nakano, A.; Yoshimatsu, A.; Uchitomi, K.; Matsuda, Y. Characterization of Molecular Aggregates of Peptide Amphiphiles and Kinetics of Dynamic Processes Performed by Single-Walled Vesicles. *J. Am. Chem. Soc.* **1984**, *106*, 3613–3623.
8. Shimizu, T.; Masuda, M.; Minamikawa, H. Supramolecular Nanotube Architectures Based on Amphiphilic Molecules. *Chem. Rev.* **2005**, *105*, 1401–1443.
9. Hartgerink, J. D.; Beniash, E.; Stupp, S. I. Self-Assembly and Mineralization of Peptide-Amphiphile Nanofibers. *Science* **2001**, *294*, 1684–1688.
10. Li, L.-S.; Jiang, H.; Messmore, B. W.; Bull, S. R.; Stupp, S. I. A Torsional Strain Mechanism to Tune Pitch in Supramolecular Helices. *Angew. Chem., Int. Ed.* **2007**, *46*, 5873–5876.
11. Ghadiri, M. R.; Granja, J. R.; Buehler, L. K. Artificial Transmembrane Ion Channels from Self-Assembling Peptide Nanotubes. *Nature* **1994**, *369*, 301–304.
12. Rajangam, K.; Behanna, H. A.; Hui, M. J.; Han, X. Q.; Hulvat, J. F.; Lomasney, J. W.; Stupp, S. I. Heparin Binding Nanostructures to Promote Growth of Blood Vessels. *Nano Lett.* **2006**, *6*, 2086–2090.
13. Lim, Y.,-b.; Park, S.; Lee, E.; Jeong, H.; Ryu, J.-H.; Lee, M. S.; Lee, M. Glycoconjugate Nanoribbons from the Self-Assembly of Carbohydrate-Peptide Block Molecules for Controllable Bacterial Cell Cluster Formation. *Biomacromolecules* **2007**, *8*, 1404–1408.
14. Sun, G.; Chu, C.-C. Self-Assembly of Chemically Engineered Hydrophilic Dextran into Microscopic Tubules. *ACS Nano* **2009**, *3*, 1176–1182.

15. Gazit, E. A Possible Role for π-Stacking in the Self-Assembly of Amyloid Fibrils. *FASEB J.* **2002**, *16*, 77–83.
16. Azriel, R.; Gazit, E. Analysis of the Minimal Amyloid-Forming Fragment of the Islet Amyloid Polypeptide: An Experimental Support for the Key Role of the Phenylalanine Residue in Amyloid Formation. *J. Biol. Chem.* **2001**, *276*, 34156–34161.
17. Kayed, R.; Bernhagen, J.; Greenfield, N.; Sweimeh, K.; Brummer, H.; Voelter, W.; Kapurniotu, A. Conformational Transitions of Islet Amyloid Polypeptide (IAPP) in Amyloid Formation *in Vitro*. *J. Mol. Biol.* **1999**, *287*, 781–796.
18. John, G.; Masuda, M.; Okada, Y.; Yase, K.; Shimizu, T. Nanotube Formation from Renewable Resources *via* Coiled Nanofibers. *Adv. Mater.* **2001**, *13*, 715–718.
19. John, G.; Jung, J. H.; Masuda, M.; Shimizu, T. Unsaturation Effect on Gelation Behavior of Aryl Glycolipids. *Langmuir* **2004**, *20*, 2060–2065.
20. Kawasaki, T.; Tokuhiro, M.; Kimizuka, N.; Kunitake, T. Hierarchical Self-Assembly of Chiral Complementary Hydrogen-Bond Networks in Water: Reconstitution of Supramolecular Membranes. *J. Am. Chem. Soc.* **2001**, *123*, 6792–6800.
21. Shiraki, T.; Morikawa, M.; Kimizuka, N. Amplification of Molecular Information Through Self-Assembly: Nanofibers Formed from Amino Acids and Cyanine Dyes by Extended Molecular Pairing. *Angew. Chem., Int. Ed.* **2008**, *47*, 106–108.
22. Aime', C.; Nishiyabu, R.; Gondo, R.; Kanekob, K.; Kimizuka, N. Controlled Self-Assembly of Nucleotide-Lanthanide Complexes: Specific Formation of Nanofibers from Dimeric Guanine Nucleotides. *Chem. Commun.* **2008**, 6534–6536.
23. Iwaura, R.; Yoshida, K.; Masuda, M.; Ohnishi-Kameyama, M.; Yoshida, M.; Shimizu, T. Oligonucleotide-Templated Self-Assembly of Nucleotide Bolaamphiphiles: DNA-Like Nanofibers Edged by a Double-Helical Arrangement of A-T Base Pairs. *Angew. Chem., Int. Ed.* **2003**, *42*, 1009–1012.
24. Kato, T.; Mizoshita, N.; Kishimoto, K. Functional Liquid-Crystalline Assemblies: Self-Organized Soft Materials. *Angew. Chem., Int. Ed.* **2006**, *45*, 38–68.
25. Terech, P.; Weiss, R., G. Low Molecular Mass Gelators of Organic Liquids and the Properties of their Gels. *Chem. Rev.* **1997**, *97*, 3133–3159.
26. Iwaura, R.; Hoeben, F. J. M.; Masuda, M.; Schenning, A. P. H. J.; Meijer, E. W.; Shimizu, T. Molecular-Level Helical Stack of a Nucleotide-Appended Oligo(*p*-phenylenevinylene) Directed by Supramolecular Self-Assembly with a Complementary Oligonucleotide as a Template. *J. Am. Chem. Soc.* **2006**, *128*, 13298–13304.
27. Yagai, S.; Kinoshita, T.; Higashi, M.; Kishikawa, K.; Nakanishi, T.; Karatsu, T.; Kitamura, A. Diversification of Self-Organized Architectures in Supramolecular Dye Assemblies. *J. Am. Chem. Soc.* **2007**, *129*, 13277–13287.
28. Yagai, S.; Monma, Y.; Kawauchi, N.; Karatsu, T.; Kitamura, A. Supramolecular Nanoribbons and Nanoropes Generated from Hydrogen-Bonded Supramolecular Polymers Containing Perylene Bisimide Chromophores. *Org. Lett.* **2007**, *9*, 1137–1140.
29. Dessingou, J.; Joseph, R.; Rao, C. P. A Direct Fluorescence-on Chemosensor for Selective Recognition of Zn(II) by a Lower Rim 1,3-Di-derivative of Calix[4]arene Possessing Bis-{*N*-(2-hydroxynaphthyl-1-methylimine)} Pendants. *Tetrahedron Lett.* **2005**, *46*, 7967–7971.
30. Singhal, N. K.; Ramanujam, B.; Mariappanadar, V.; Rao, C. P. Carbohydrate-Based Switch-on Molecular Sensor for Cu(II) in Buffer: Absorption and Fluorescence Study of the Selective Recognition of Cu(II) Ions by Galactosyl Derivatives in HEPES Buffer. *Org. Lett.* **2006**, *8*, 3525–3528.
31. Ahuja, R.; Singhal, N. K.; Ramanujam, B.; Ravikumar, M.; Rao, C. P. Experimental and Computational Studies of the Recognition of Amino Acids by Galactosyl-imine and -amine Derivatives: An Attempt to Understand the Lectin−Carbohydrate Interactions. *J. Org. Chem.* **2007**, *72*, 3430–3442.
32. Kumar, A.; Singhal, N. K.; Ramanujam, B.; Mitra, A.; Rameshwaram, N. R.; Nadimpalli, S. K.; Rao, C. P. C_1-/C_2-Aromatic-imino-glyco-conjugates: Experimental and Computational Studies of Binding, Inhibition, and Docking Aspects toward Glycosidases Isolated from Soybean and Jack Bean. *Glycoconjugates J.* **2009**, *26*, 495–510.
33. Pathak, R. K.; Ibrahim, Sk.Md.; Rao, C. P. Selective Recognition of Zn^{2+} in Aqueous Acetonitrile by Salicylaldimine Appended Triazole Linked Di-derivatives of Calix[4]arene by Enhanced Fluorescence Emission: Role of Terminal−CH_2OH Moieties in Conjunction with the Imine in Recognition. *Tetrahedron Lett.* **2009**, *50*, 2730–2734.
34. Singhal, N. K.; Mitra, A.; Rajsekhar, G.; Shaikh, M. M.; Kumar, S.; Guionneau, P.; Rao, C. P. Role of the Orientation of−OH Groups on Sensitivity and Selectivity of the Interaction of M^{2+} with Ribosyl- and Galctosyl-imino-conjugates: Solution Recognition Studies of M^{2+} in MeOH and Selective Recognition of Cu^{2+} in HEPES Buffer, and First Crystal Structure Determination of Dinuclear-Cu(II) Complexes Based on Both the Glyco-imino-conjugates. *Dalton Trans.* **2009**, 8432–8442.
35. Pathak, R. K.; Dikundwar, A. G.; Guru Row, T. N.; Rao, C. P. A Lower Rim Triazole Linked Calix[4]arene Conjugate as a Fluorescence Switch on Sensor for Zn^{2+} in Blood Serum Milieu. Chem. Commun., published online May 12, 2010, http://doi.dx.org/, 10.1039/c0cc00219d.
36. Yang, H.; Pritzker, M.; Fung, S. Y.; Sheng, Y.; Wang, W.; Chen, P. Anion Effect on the Nanostructure of a Metal Ion Binding Self-Assembling Peptide. *Langmuir* **2006**, *22*, 8553–8562.
37. *Hyperchem 8.0.4*; Hypercube, Inc.: Gainesville, FL, 2007.
38. Mitra, A.; Chinta, J. P.; Rao, C. P. 1-(D-Glucopyranosyl-2′-deoxy-2′-iminomethyl)-2-hydroxybenzene as Chemosensor for Aromatic Amino Acids by Switch-on Fluorescence. *Tetrahedron Lett.* **2010**, *51*, 139–142.
39. Edwards, J. V., Buschle-Diller, G., Goheen, S. C. Modified Fibers with Medical and Specialty Applications. Goheen, S. C., Edwards, J. V., Rayburn, A., Gaither, K, Castro, N., Eds.; Springer: The Netherlands, 2006; pp 49−65.
40. Lu, K.; Jacob, J.; Thiyagarajan, P.; Conticello, V. P.; Lynn, D. G. Exploiting Amyloid Fibril Lamination for Nanotube Self-Assembly. *J. Am. Chem. Soc.* **2003**, *125*, 6391–6393.